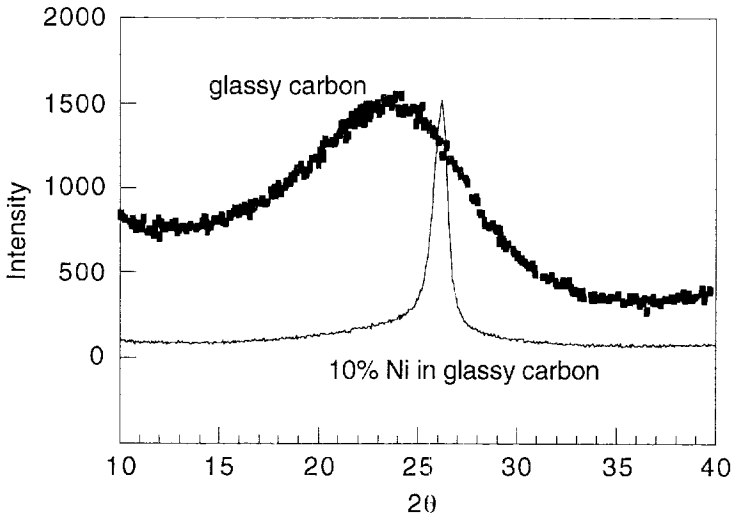

Fig. 33. XRD [002] diffraction peaks of glassy carbon with and without 10% Ni. Samples annealed at 1000°C for 100 h.

dusting of Ni is similar to that for Fe, except that no precipitation of Ni carbide is observed, and carbon diffusion and crystallization of coke on the underside of the metal surface, which enable separation of Ni particles, govern the process.

Behavior of Fe- and Ni-Base Alloys

Table 3 lists the chemical compositions of Fe- and Ni-base alloys that were selected for study. Several of the screening tests (Runs 1 through 9 listed in Table 4) were used to establish the testing conditions for long-term experiments with Fe- and Ni-base alloys (Runs 11-27 in Table 4). One of the important results was that the Fe- and Ni-base alloys should not be exposed in the same run simultaneously, since the Fe-base alloys exhibited a carbon deposit much earlier than the Ni-base alloys, and significant cross contamination between these classes of alloys occurred. Furthermore, the Fe-base alloys with lower Cr contents (e.g., T22) were much more susceptible to carbon deposition and metal dusting attack when exposed under the same temperature, time, and gas composition.

Runs 11 through 14 were conducted to isolate the Fe and Ni specimens during exposure and also to evaluate the influence of H_2O in the exposure environment on the carbon deposition and dusting processes. Runs 15 and 16 were of 1000-h duration and were conducted with Fe- and Ni-base alloys in Gas 2, which simulated the reformer effluent. This gas contained 23 vol.% H_2O, which was achieved by pumping water into the reaction chamber through a specially designed heater. Runs 17 and 18 were conducted to evaluate the carbon deposition/dusting behavior at 482°C (900°F).

Detailed analysis of the specimens from Runs 15 and 16 showed little, if any, deposit of carbon on the specimen surfaces. Carbon was noted primarily on the T22 specimen, and virtually no carbon was detected in Run 16 coincident with Ni-base alloys. The major difference between these runs and the others (Runs 1 through 9) was the amount of H_2O in the exposure environment. Note that the carbon activity established by Gas 2 at 593°C (1100°F) is >2 (see Table 3), yet no deposit of carbon was noted.

Run 19 was conducted to examine the competing effects of oxidation and carbon deposition/metal dusting on alloy behavior. In this run, Fe-base alloys were exposed in Gas 2, but in contrast to Run 15, with only 2 vol.% H_2O. The calculated values for carbon activity in runs 15 and 19 were 2 and 30, respectively, at 593°C (1100°F). In Run 19, a copious amount of carbon was observed on specimen surfaces. Figure 34 shows a macroscopic photograph of the specimens exposed in Runs 15 and 19.

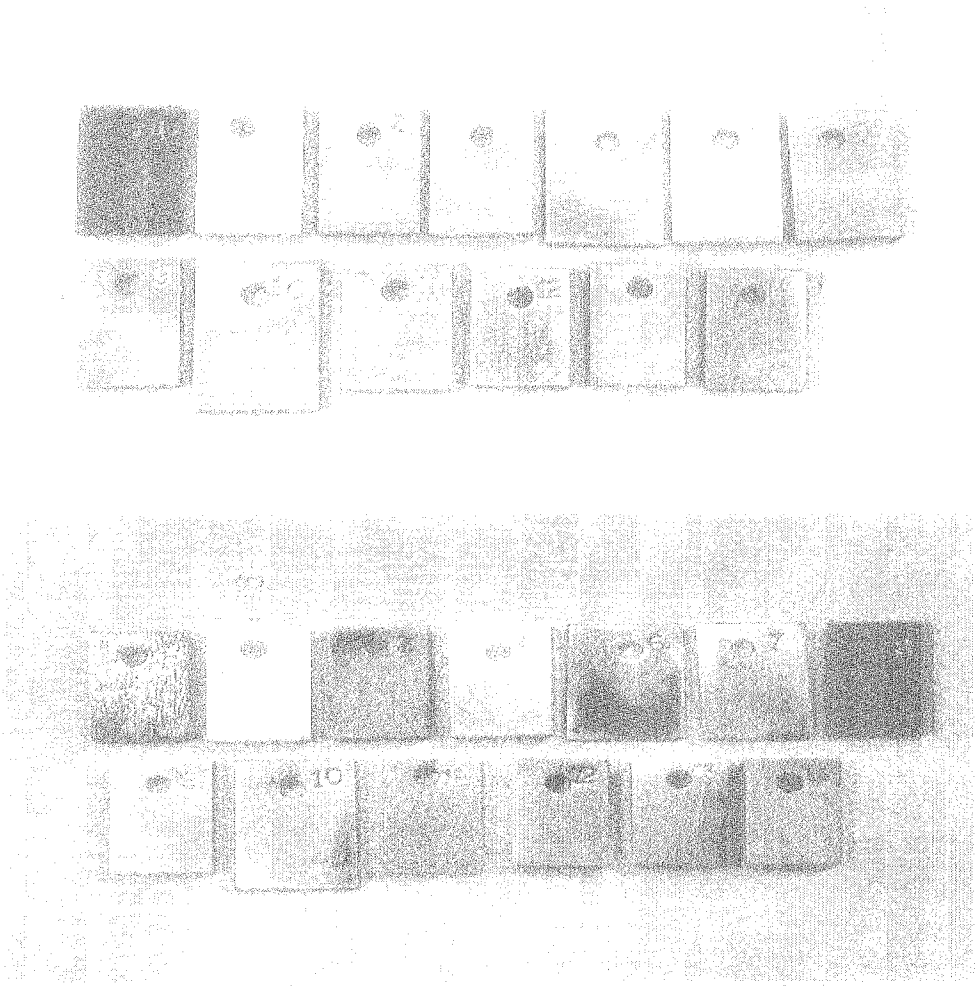

Fig. 34. Macrophotographs of Fe-base alloy specimens after 1000-h exposure at 593°C (1100°F) in Run 15 in Gas 2 with 23.1 vol.% H_2O (top) and Run 19 in Gas 2 with 2 vol.% H_2O (bottom).

Detailed analysis of the surfaces of specimens exposed in Runs 15 and 16 indicated development of oxide layers on most of the specimens. Figures 35–37 show SEM photomicrographs of surfaces of several Fe-base alloys after 1000-h exposure in Gas 2 at 593°C (1100°F). In general, most of the alloys exhibited oxide scales on the surface; however, at isolated locations some carbon deposit adhered to the surface. No significant pitting-type attack was noted in any of the high-Ni specimens. The only alloy that exhibited a copious amount of carbon deposit and metal dusting was T91 steel, which contained 0.25 wt.% C. Figure 38 shows SEM photomicrographs of several alloys in higher magnification; alloys MA956 and APMT (which contained 6.5 and 4.9 wt.% Al, respectively) developed thin alumina scales, whereas alloys 253MA and 353MA only developed chromia or (Fe,Cr) oxide scales, even though they contained 1.6 and 5.8 wt.% Si, respectively.

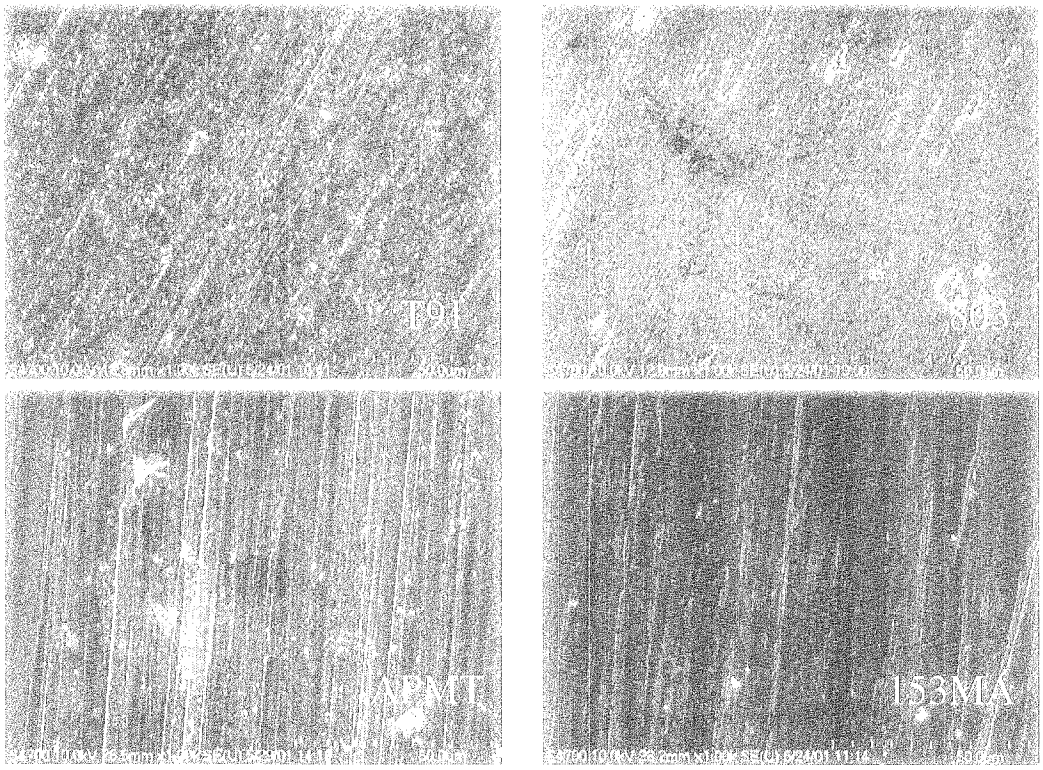

Fig. 38. SEM photomicrographs of surfaces of (top left) T91, (top right) 800H, (bottom left) APMT, and (bottom right) 153MA after 1000-h exposure in Run 16.

Figures 39 and 40 show SEM photomicrographs of surfaces of several Ni-base alloys after 1000-h exposure in Gas 2 at 593°C (1100°F). In general, Ni-base alloys develop much thinner oxide scales than the Fe-base alloys. However, carbon adherence onto the surface of Ni-base alloy is much stronger, as evidenced by the presence of it even after prolonged ultrasonic cleaning. Furthermore, the carbon deposit can be seen as striations, forming preferentially along the polishing lines on the surface. Also, a nonuniform distribution of carbon is evident.

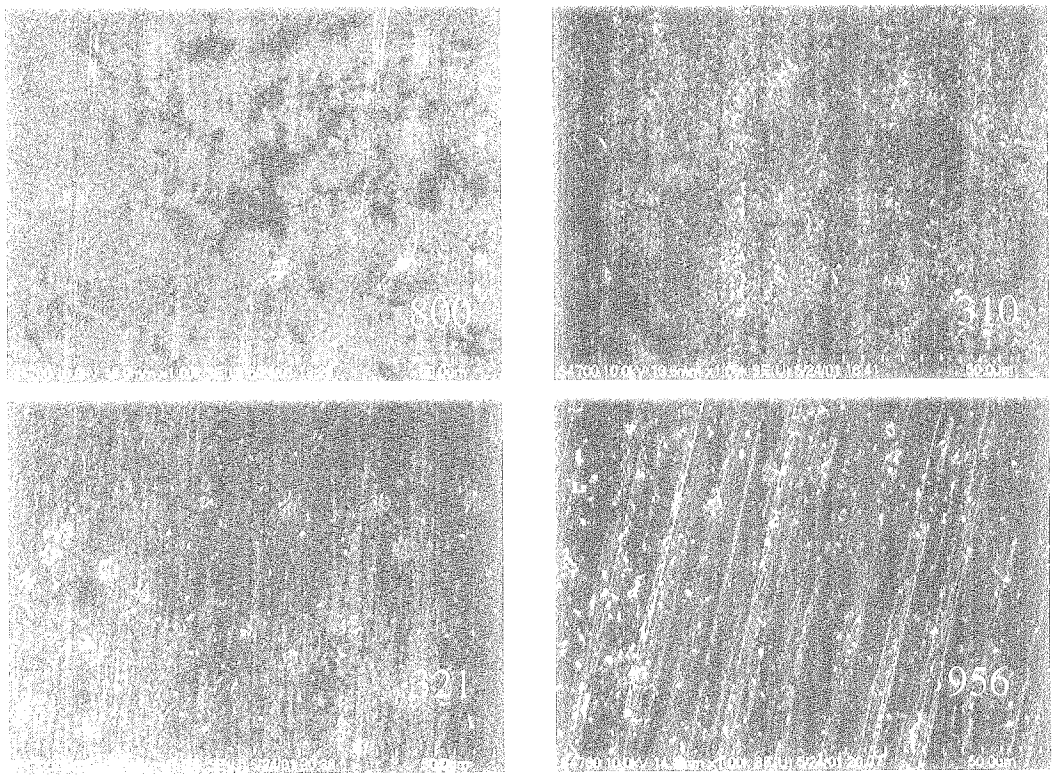

Fig. 36. SEM photomicrographs of surfaces of (top left) Alloy 800, (top right) 310 SS, (bottom left) 321 SS, and (bottom right) MA956 after 1000-h exposure in Run 15.

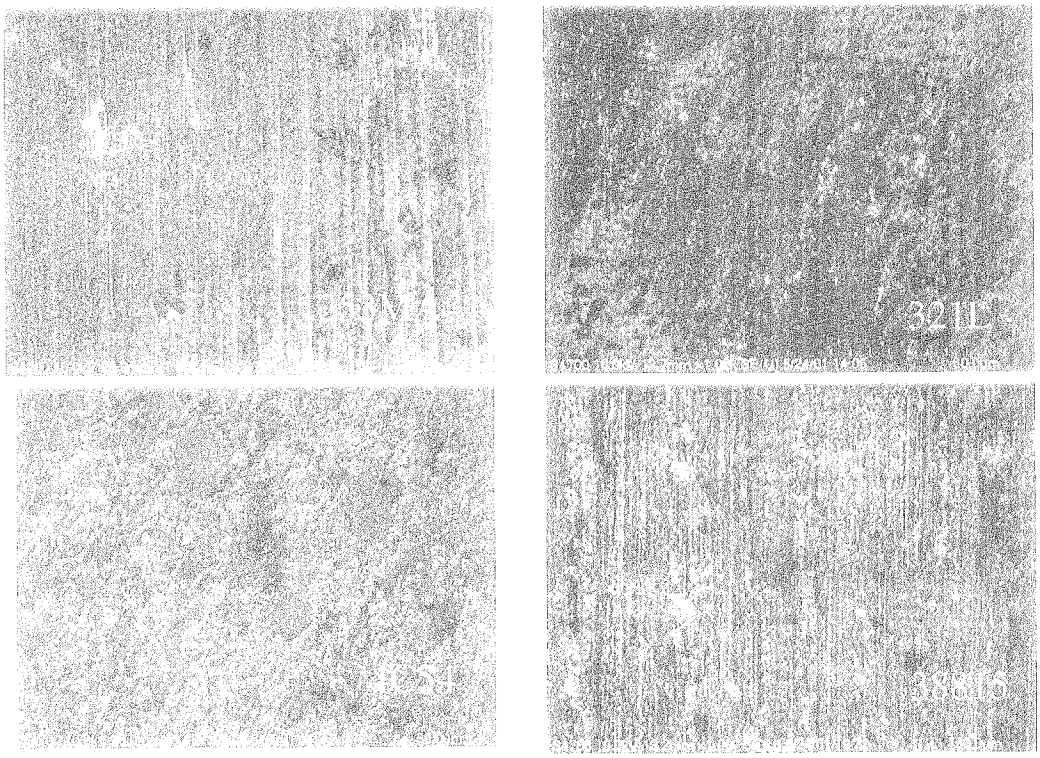

Fig. 37. SEM photomicrographs of surfaces of (top left) 253MA, (top right) 321L, (bottom left) 4C54, and (bottom right) 38815 after 1000-h exposure in Run 15.

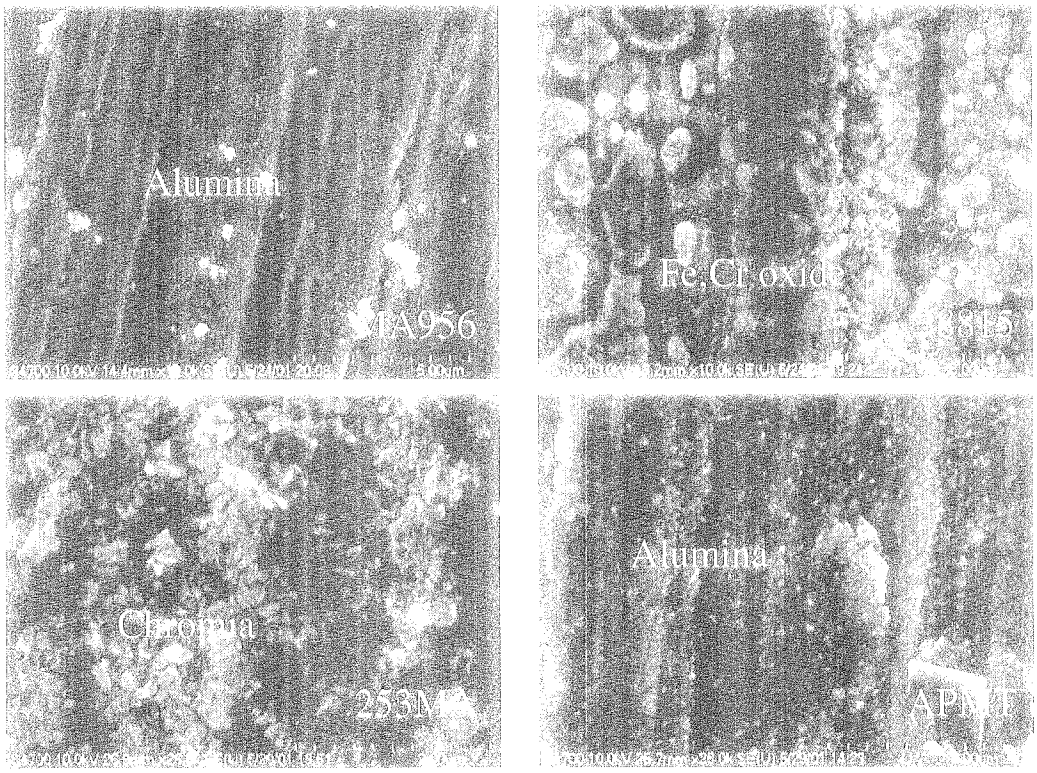

Fig. 38. Higher magnification SEM photomicrographs of surfaces of (top left) MA956, (top right) 316L, (bottom left) 253MA, and (bottom right) APMT after 1000-h exposure in Run 15.

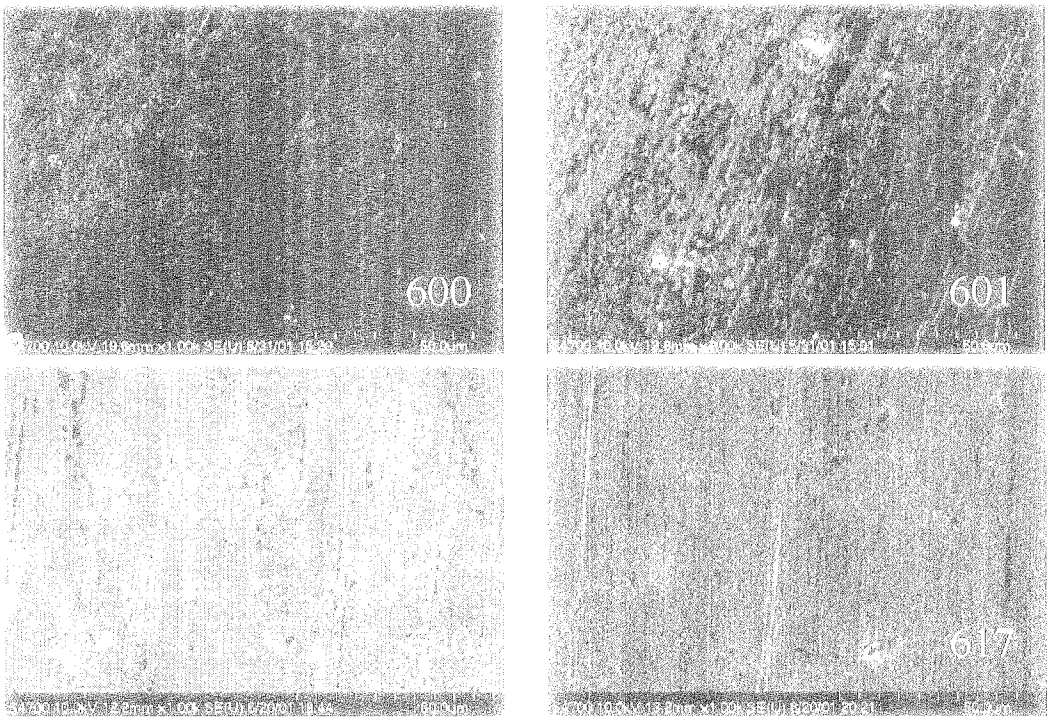

Fig. 39. SEM photomonographs of surfaces of (top left) 600, (top right) 601, (bottom left) 690, and (bottom right) 617 after 1000-h exposure in Run 16.

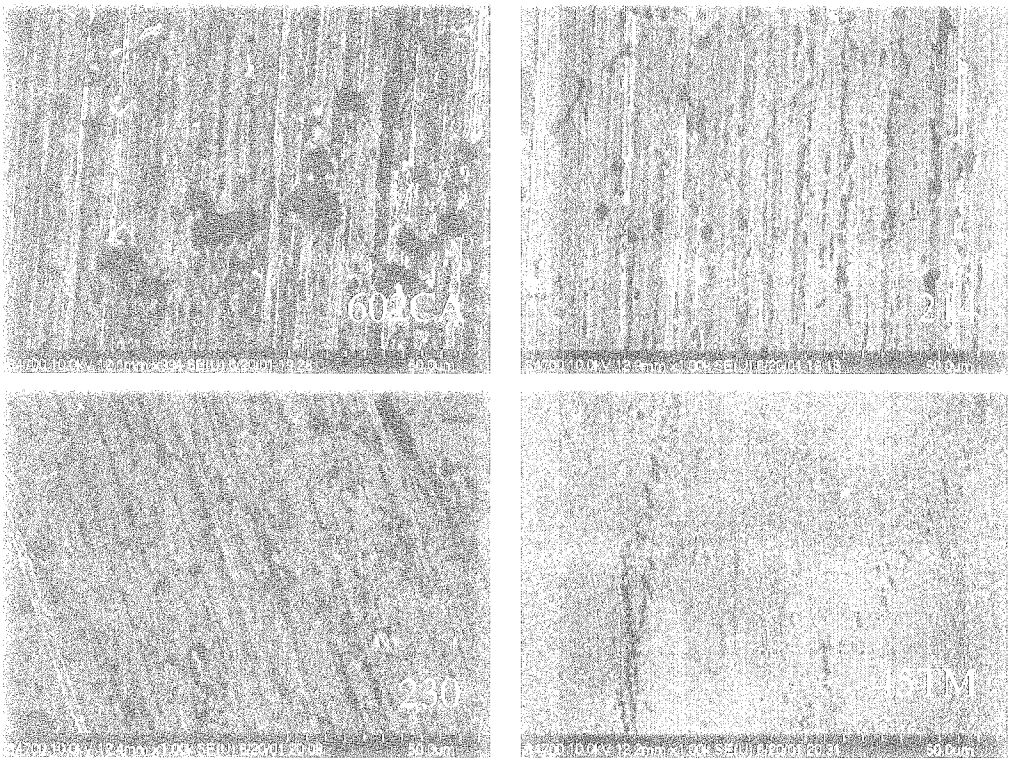

Fig. 40. SEM photomicrographs of surfaces of (top left) 602CA, (top right) 214, (bottom left) 230, and (bottom right) 45TM after 1008-h exposure in Run 16.

To examine the carbon penetration, if any, into the alloys, several of the exposed specimens were cut, mounted, polished, and cross sectioned for SEM and EDX analyses. Figures 41 and 42 show the SEM photomicrographs of cross sections of several Fe- and Ni-base alloys, respectively, after 1008-h exposure in the metal dusting environment. 214 alloy developed a thin oxide scale and virtually no carbon penetration, even after 1008-h exposure. The oxide scale developed on Alloy 800 was porous and discontinuous, and several pits have initiated from the surface (see Fig. 41). Alloy 32 developed a thin oxide scale with almost no carbon penetration into the alloy, indicating that the soot of carbon observed on the surface (see Fig. 36) are primarily adherent to the thin oxide layer.

Among the Ni base alloys that were exposed in Run 16, Alloys 600, 690, 602CA, and 45TM were examined in cross section. Figure 42 shows the SEM photomicrographs of these specimens. The scales were continuous and adherent to the substrate and the thickness was 0.1–0.5 μm after 1008-h exposure in Gas 2 at 593°C (1100°F). None of the alloys exhibited internal penetration of carbon or pitting attack.

Raman spectroscopy was used to analyze the carbon that adhered to the surface of Fe- and Ni-base alloys exposed in Runs 15 and 16. Figure 43 shows Raman spectra (frequency range 1000–1700 cm^{-1}) for carbon that adhered to the surface of alloys 122,

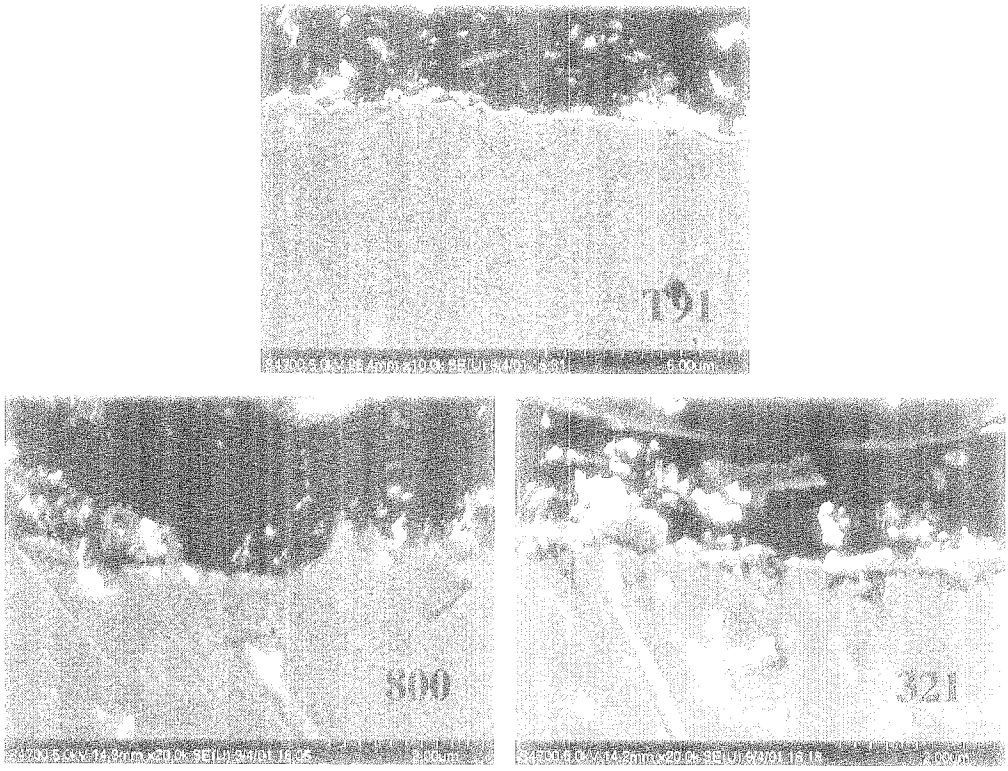

Fig. 41. SEM photomicrographs of cross sections of (top) T91, (bottom left) 800, and (bottom right) 321 after 1000-h exposure in Run 15.

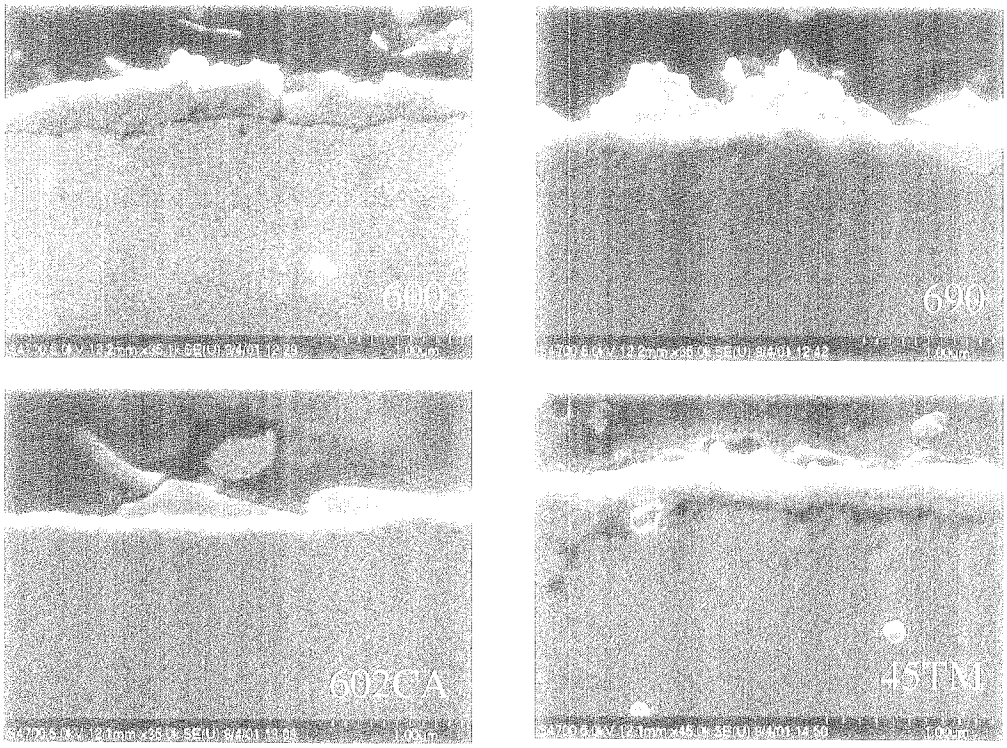

Fig. 42. SEM photomicrographs of cross sections of (top left) 600, (top right) 690, (bottom left) 602CA, and (bottom right) 45TM after 1000-h exposure in Run 15.

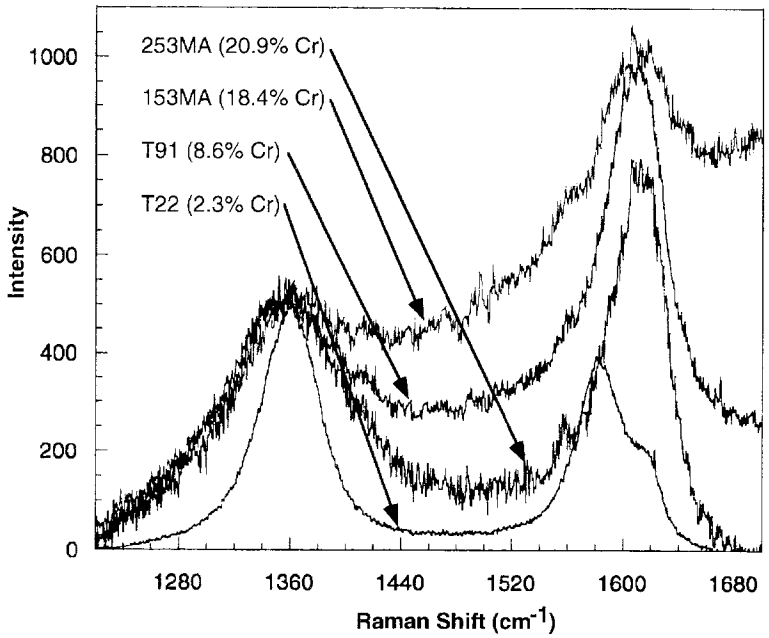

Fig. 43. Raman spectra for carbon adhered to several alloys with different Cr contents after 1000-h exposure in a metal dusting environment in Run 15 at 593°C (1100°F).

T91, 153MA, and 253MA (which had Cr contents of 2.25, 8.6, 18.4, and 20.9, respectively). The alloy T22, which exhibited severe metal dusting attack, had much sharper peaks of carbon when compared with those for the other alloys. Figure 44 shows the Raman spectra (frequency range 200-800 cm^{-1}) for the same Fe-base alloys with different Cr contents, after 1000-h exposure in the metal dusting environment in Run 15 at 593°C (1100°F). The Raman spectra in the frequency range 200-800 cm^{-1} clearly show that alloys with Cr >8.6 wt.% develop oxide scales, as evidenced by the SEM photomicrographs presented earlier. The peaks at ≈550 and ≈680 cm^{-1} correspond to Cr_2O_3 and (Fe,Cr) oxide spinel, respectively. Lack of oxide scale on alloy T22 (which contained 2.3 wt.% Cr) led to metal dusting attack during the 1000-h exposure in Run 15.

Figure 45 shows the Raman spectra (frequency range 200-800 cm^{-1}) for the three Ni-base alloys with different Cr contents after 1000-h exposure in the metal dusting environment in Run 16 at 593°C (1100°F). The Ni-base alloys predominantly developed Cr_2O_3, as indicated by the peak at ≈550 cm^{-1}. The peak height seems to be strongly dependent on the Cr content of the alloy; for example, among the three alloys the peak height is smallest for Alloy 600 (15.4 wt.% Cr) and largest for Alloy 690 (27.2 wt.% Cr). The broad feature in these spectra at ≈660 cm^{-1} is not currently identified but seems to disappear as the Cr level in the alloy increases.

Figures 46 and 47 show the Raman spectra in the frequency ranges of 200-800 cm^{-1} and 1200-1800 cm^{-1}, respectively, for Fe-base alloys with variation in Cr content. All

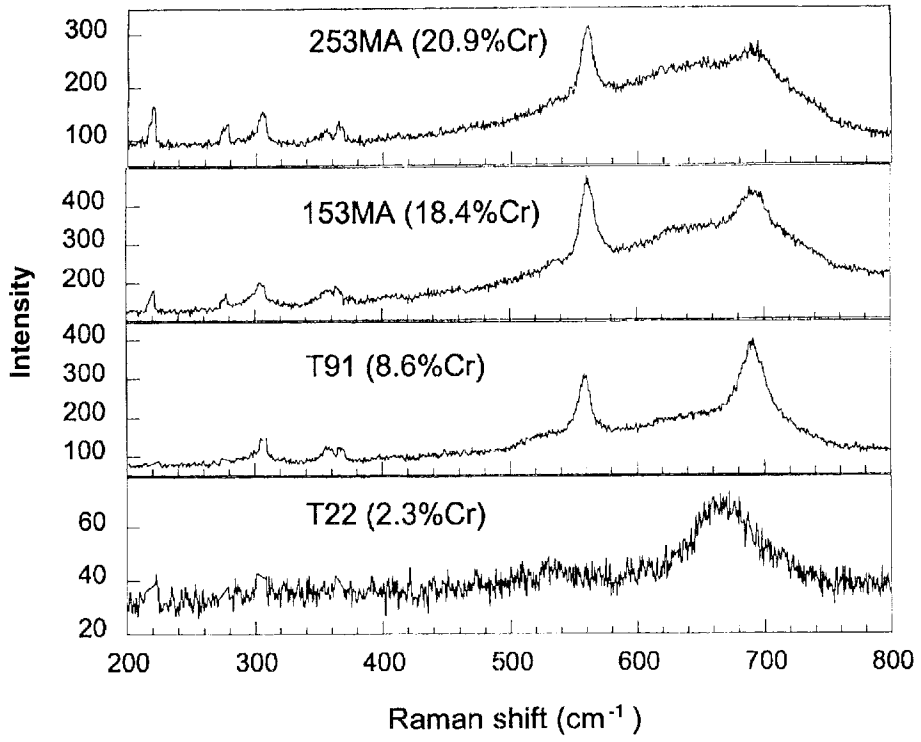

Fig. 44. Raman spectra for surfaces of several Fe-base alloys with different Cr contents after 1000-h exposure in a metal dusting environment in Run 15 at 593°C (1100°F).

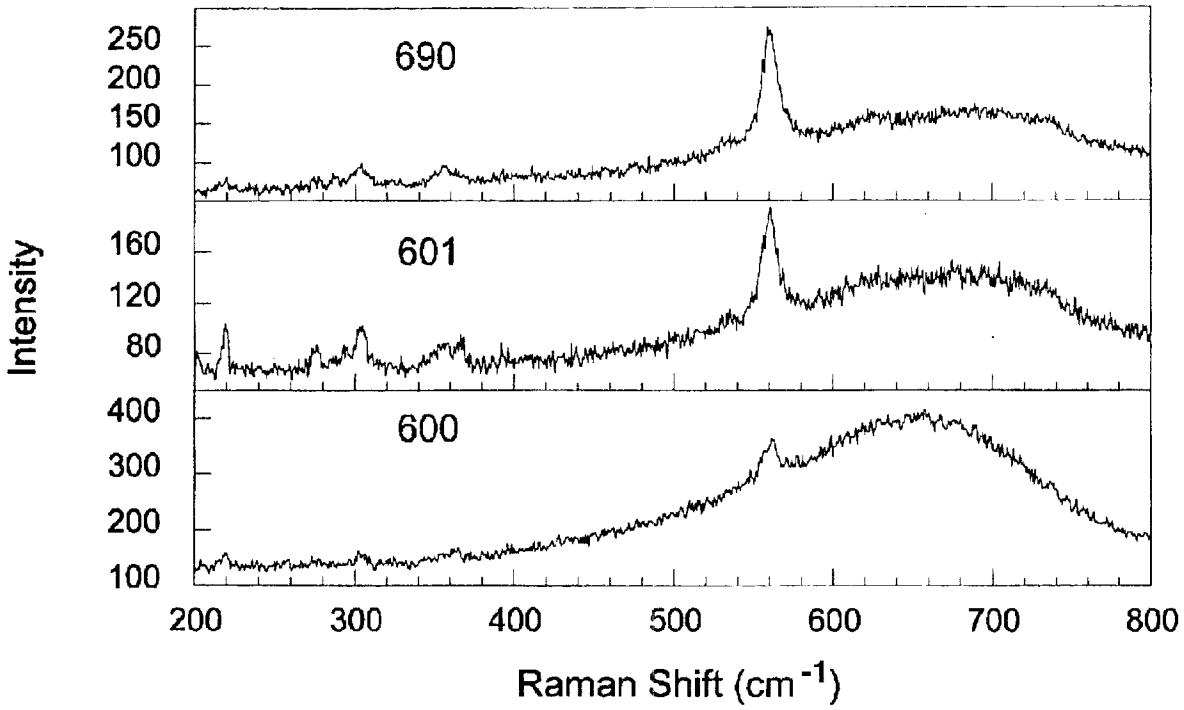

Fig. 45. Raman spectra for surfaces of several Ni-base alloys with different Cr contents after 1000-h exposure in a metal dusting environment in Run 16 at 593°C (1100°F).

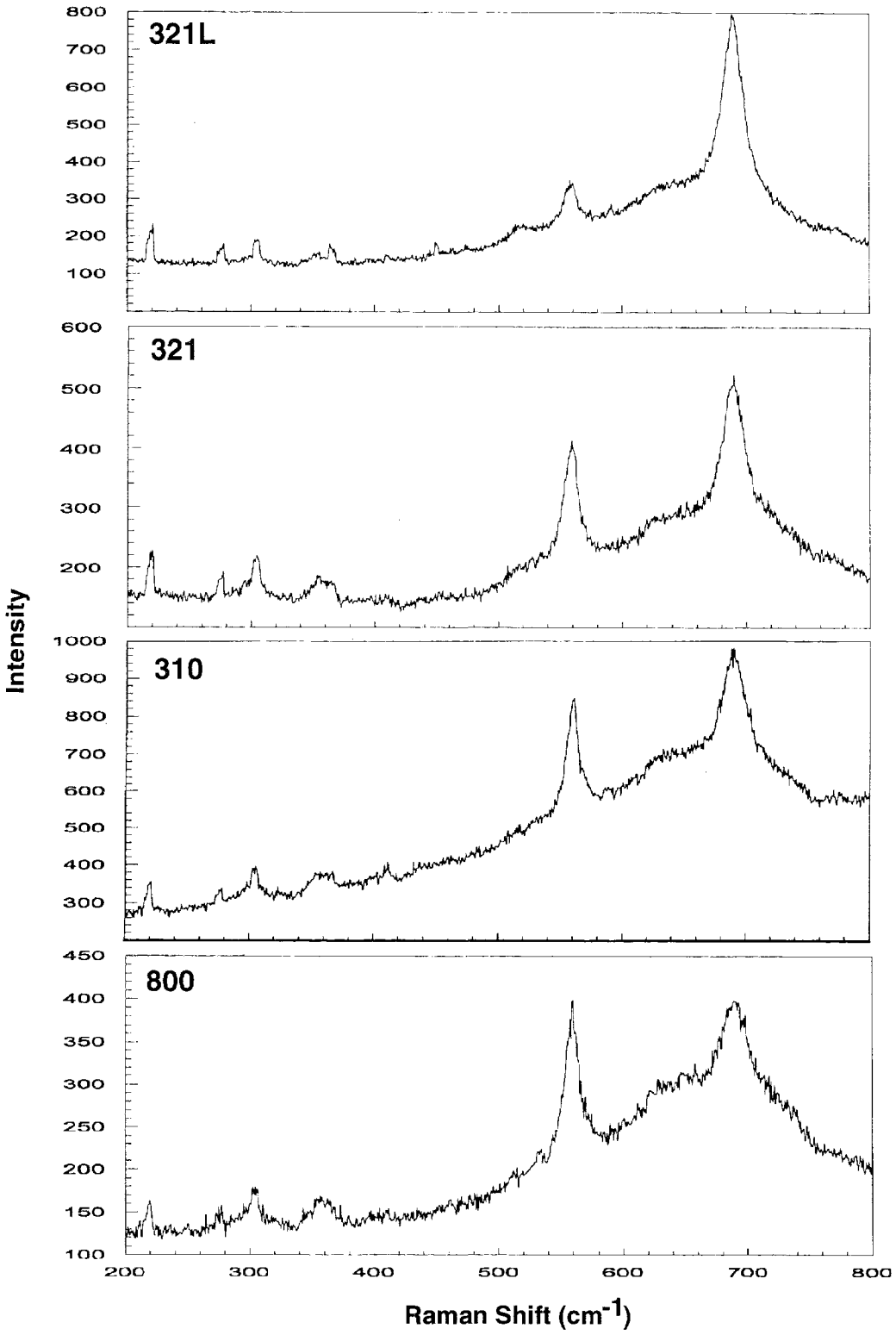

Fig. 46. Raman spectra (frequency range 200-800 cm^{-1}) for surfaces of 300-series stainless steel alloys and Alloy 800 after 1000-h exposure in a metal dusting environment at 593°C (1100°F).

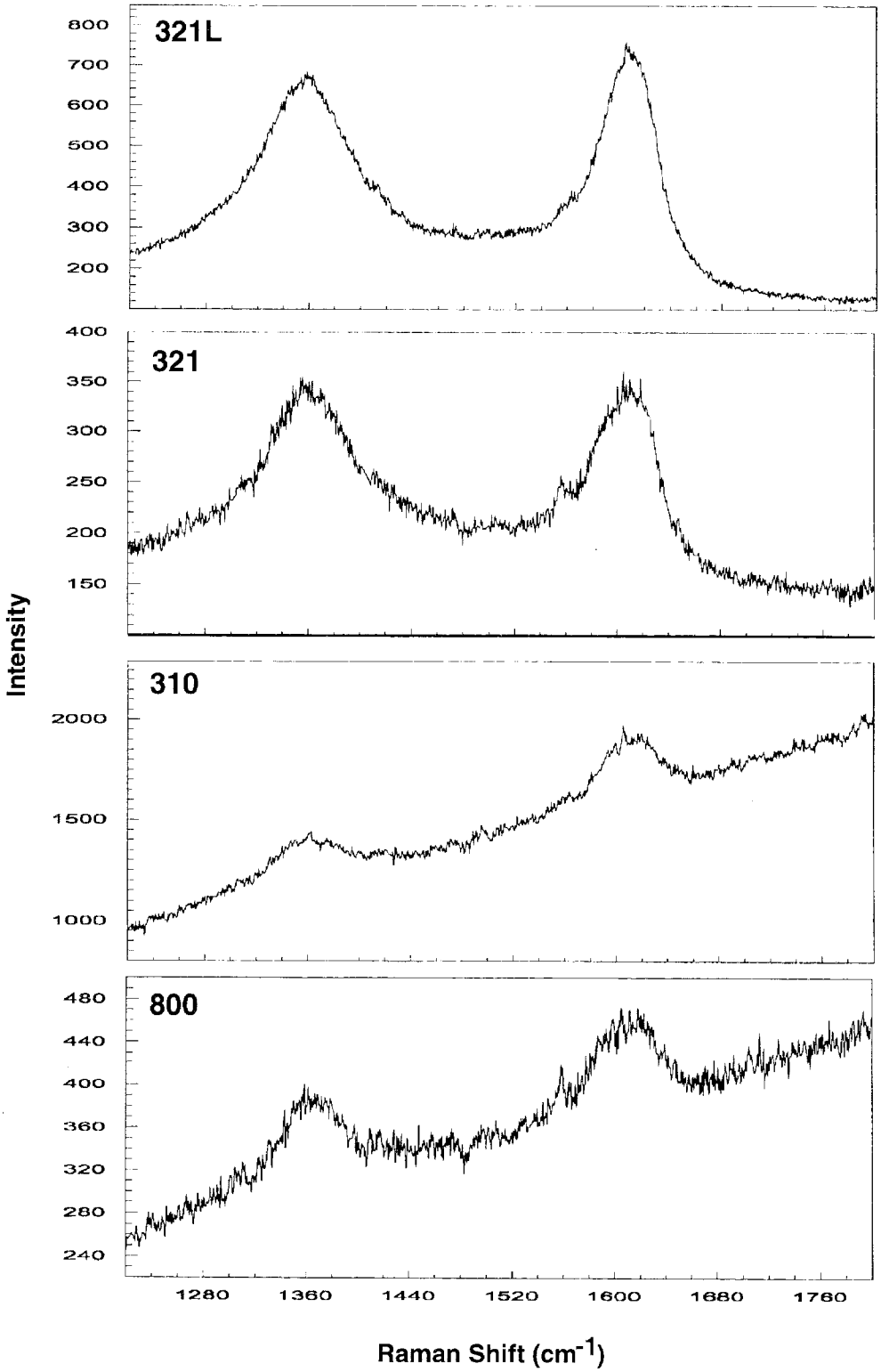

Fig. 47. Raman spectra (frequency range 1200-1800 cm^{-1}) for surfaces of 300-series stainless steel alloys and Alloy 800 after 1000-h exposure in a metal dusting environment at 593°C (1100°F).